PHYSICAL REVIEW B **89**, 174415 (2014)

Spin-liquid phase due to competing classical orders in the semiclassical theory of the Heisenberg model with ring exchange on an anisotropic triangular lattice

Michael Holt,[1] Ben J. Powell,[1] and Jaime Merino[2]
[1]*Centre for Organic Photonics and Electronics, School of Mathematics & Physics, University of Queensland, Brisbane, Queensland 4072, Australia*
[2]*Departamento de Física Teórica de la Materia Condensada, Condensed Matter Physics Center (IFIMAC) and Instituto Nicolás Cabrera, Universidad Autónoma de Madrid, Madrid 28049, Spain*
(Received 11 July 2013; revised manuscript received 3 April 2014; published 13 May 2014)

We investigate the effect of ring exchange on the ground-state properties and magnetic excitations of the $S = 1/2$ Heisenberg model on the anisotropic triangular lattice with ring exchange at $T = 0$ using linear spin-wave theory. Classically, we find stable Néel, spiral and collinear magnetically ordered phases. Upon including quantum fluctuations to the model, linear spin-wave theory shows that ring exchange induces a large quantum disordered region in the phase diagram, completely wiping out the classically stable collinear phase. Analysis of the spin-wave spectra for each of these three models demonstrates that the large spin-liquid phase observed in the full model is a direct manifestation of competing classical orders. To understand the origin of these competing phases, we introduce models where either the four spin contributions from ring exchange, or the renormalization of the Heisenberg terms due to ring exchange are neglected. We find that these two terms favor rather different physics.

DOI: 10.1103/PhysRevB.89.174415 PACS number(s): 75.10.Kt, 75.10.Jm, 75.30.Ds, 75.50.Ee

I. INTRODUCTION

Quantum spin liquids are characterized by ground states with no long-range magnetic order and no breaking of spatial (rotational or translational) symmetries that are not adiabatically connected to the band insulator [1–3]. Recently, a number of experiments have identified a handful of materials as candidate spin liquids [4–14]. Both the organic charge transfer salts κ-(BEDT-TTF)$_2$Cu$_2$(CN)$_3$ (Refs. [5–8]) and Me$_3$EtSb[Pd(dmit)$_2$]$_2$ (Refs. [8–10]), where Et = C$_2$H$_5$ and Me = CH$_3$ are spin-liquid candidates. However, other members of the organic charge transfer salt families κ-(BEDT-TTF)$_2X$ and Y[Pd(dmit)$_2$]$_2$ display long-range magnetic order, for example, X = Cu[N(CN)$_2$]Cl or Cu[N(CN)$_2$]Br (for deuterated BEDT-TTF) and Y = Me$_4$P, Me$_4$As, EtMe$_3$As, Et$_2$Me$_2$P, Et$_2$Me$_2$As, and Me$_4$Sb [3,8,11]. Additionally, the inorganic materials Cs$_2$CuCl$_4$ [12], Ba$_3$CoSb$_2$O$_9$ [13], and Ba$_3$CuSb$_2$O$_9$ [14] have also been suggested to be spin-liquid candidates.

The simplest model for the Mott insulating states of the κ-(BEDT-TTF)$_2X$ and Y[Pd(dmit)$_2$]$_2$ salts is the half-filled Hubbard model on the anisotropic triangular lattice [3] [see Fig. 1(a)], where each site represents a dimer, (BEDT-TTF)$_2$ or [Pd(dmit)$_2$]$_2$. This model contains three parameters: U the effective on-site Coulomb repulsion, t the nearest-neighbor hopping integral, and t' the next-nearest-neighbor hopping integral along one diagonal only. The Hubbard model on the anisotropic triangular lattice has been studied via a number of approaches [15–21]. Some methods have suggested that a spin liquid is realized in the insulating phase.

For $U \gg t,t'$, i.e., deep in the Mott insulating phase, the model simplifies further to the Heisenberg model on the anisotropic triangular lattice with $J = 4t^2/U$ and $J' = 4t'^2/U$ to leading order. Electronic structure calculations on the anisotropic triangular lattice [22–26] suggest that both spin liquids κ-(BEDT-TTF)$_2$Cu$_2$(CN)$_3$ and Me$_3$EtSb[Pd(dmit)$_2$]$_2$ and the valence bond solid, Me$_3$EtP[Pd(dmit)$_2$]$_2$, have $0.5 \lesssim J'/J \lesssim 0.8$; whereas salts that display long-range order have either $J'/J \lesssim 0.5$ or $J'/J \gtrsim 0.8$. The anisotropic triangular lattice is also realized in Cs$_2$CuBr$_4$ ($J'/J \approx 2$) and Cs$_2$CuCl$_4$ ($J'/J \approx 3$) [12] and the isotropic limit ($J'/J = 1$) describes Ba$_3$CoSb$_2$O$_9$ and Ba$_3$CuSb$_2$O$_9$ [27].

Many of the organic charge transfer salts considered here undergo Mott metal-to-insulator transitions under relatively modest hydrostatic pressures [8,28]. This suggests that higher order terms in the U/t expansion may be relevant. Furthermore, there is significant variation in the critical pressure required to drive the Mott transition in different salts [29], which suggests that different salts represent different values of U/t and not just different values of t'/t. There has been far less investigation of how U/t affects the properties of the materials than t'/t. If one continues to integrate out the charge degrees of freedom, the first nontrivial new terms appear at fourth order with the "ring-exchange" processes illustrated in Fig. 1(b) [see also Eq. (1), below]. Such ring exchange processes frustrate the system. There are two distinct ring exchange terms on the anisotropic triangular lattice $K = 80t^4/U^3$ and $K' = 80t^2t'^2/U^3$ to lowest order [30,31], which originate from the different ways to arrange four-sites on the anisotropic triangular lattice. Note that the large prefactor means that the ring exchange term is relevant to larger values of U/t than one would expect naïvely. It has been argued [32,33] that near the Mott transition ring exchange destroys the long-range magnetic order. In particular, for $J' = J$ and $K' = K$ Motrunich [32] found that AFM order is preserved for small $K/J \lesssim 0.14$–0.20 [34] but is destroyed for larger K/J leading to a gapped spin liquid for $K/J > 0.28$. However, this implies that applying pressure, which decreases U/t, should drive a magnetically ordered to spin-liquid transition, which has not been observed in the antiferromagnetically ordered organic charge transfer salts with $t' \simeq t$.

The isotropic triangular lattice with multiple-spin exchange has been widely studied since the 1960s in the context of

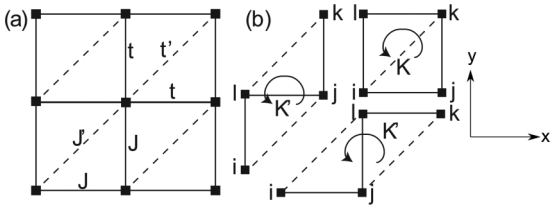

FIG. 1. (a) Sketch of the anisotropic triangular lattice showing the exchange interactions J and J', which act in the nearest neighbor and next-nearest neighbor along one diagonal directions as shown. (b) The three distinct ways to draw the four-site plaquettes relevant to ring exchange on the anisotropic triangular lattice. We have also shown the x-y coordinate system in which we perform our analysis.

solid ^{3}He; for an extensive review of magnetism in solid ^{3}He, see Roger [35] and references therein. Since the early studies by Thouless [36], single monolayers of solid ^{3}He have been absorbed on graphite [37,38] and several studies were performed to develop a theoretical understanding of the experiments in terms of multiple spin-exchange models [39–47]. Additionally, multiple spin-exchange models have gained interest in frustrated spin systems, in particular the parent cuprate high-temperature superconductors [48–50].

The Heisenberg model on the isotropic triangular lattice without ring exchange ($J' = J, K = K' = 0$) has been studied extensively [1,3]. Anderson first proposed the resonating valence bond (RVB) spin-liquid state as a possible ground state of the isotropic triangular lattice [51]. However, later numerical work [52] has shown that the ground state has "120° order"—a special case of spiral order, discussed below, with an ordering wave vector $\mathbf{Q} = (2\pi/3, 2\pi/3)$. A range of other methods have been used to study the Heisenberg model on the anisotropic triangular lattice including linear spin-wave theory [53,54], modified spin-wave theory [55], series expansions [12,56], the coupled cluster method [57], large-N expansions [58], variational Monte Carlo [59], resonating valence bond theory [15,19,60–62], pseudofermion functional renormalization group [63], slave rotor theory [64], renormalization group [65], and the density matrix renormalization group [66]. These calculations show that for small J'/J, Néel (π,π) order is realised and spiral (q,q) long-range AFM order is realized for $J'/J \sim 1$. There remains controversy as to whether another state is realized between these two phases, but no conclusive evidence for a spin-liquid ground state has been found in this model.

The only works we are aware of to discuss the Heisenberg model on the anisotropic triangular lattice with ring exchange consider two-leg [67] and four-leg [68] ladders. Both studies suggest the existence of quantum spin liquids. Therefore it is important to ask how these states survive as one moves to the full two-dimensional problem.

Hauke [55,69] has considered the fully anisotropic triangular lattice and argued that this can explain the phase diagram of the organic charge transfer salts. Alternative models such as the quarter-filled Hubbard model, with each site representing a monomer [70] and multiorbital models [25] have also been proposed. These works do not consider ring exchange and it is believed that additional interaction terms beyond the nearest neighbor Heisenberg model need to be included to help understand and explain why some materials have magnetically ordered or spin-liquid ground states.

Very recently we studied the effect of third nearest-neighbor interactions within a mean-field Schwinger-boson framework [71] and found a spin-liquid phase for $J'/J > 1.8$ and $J_3/J \lesssim 0.1$. Such terms can arrive as the two-spin contribution from ring exchange. Majumdar *et al.* [72] has performed a spin-wave theory study to order $1/S^2$ of the effect of ring exchange on the Néel phase, but only considered the four-spin terms and neglected the two-spin renormalization. It is therefore interesting to study the effect of the full ring-exchange term on the observed magnetic properties of the anisotropic triangular lattice.

The aim of the present work is to investigate the effect of ring exchange on the magnetic properties of the anisotropic triangular lattice, using linear spin-wave theory. Linear spin-wave theory provides an important benchmark and is a good starting point for more technical studies. Furthermore, we will explicitly compare the behavior of the model keeping only spin-exchange or four-spin exchange terms from ring exchange with the full model considering both exchange terms.

For the full model, we found Néel order is robust to ring exchange for $J'/J \ll 1$, being stable up to around $J'/J \approx 0.59$ for $K/J \approx 0.12$. For $K/J > 0.12$, minima develop along the (k,k) direction which cause the Néel order to become destabilized. We also found that the spiral phase was dramatically suppressed in the quantum calculations. With strong quantum fluctuations, the spiral phase was only able to survive up to $K/J = 0.10$ for $J'/J = 1$ in contrast to $K/J = 1/3$ found classically. In the weakly-coupled chain limit of our model $J'/J \gg 1$, we found spiral order persists in the presence of weak frustration from ring exchange ($K'/K \ll 1$). This is highly analogous to the "order-by-disorder" mechanism due to quantum or thermal fluctuations [73–75]. In a large region of the quantum phase diagram, the classically stable collinear phase is wiped out and replaced with a spin-liquid phase. Analysis of the spin-wave spectra show that the spin liquid is a consequence of competition between classical ordered states.

The present work is organised as follows. In Sec. II, we introduce the anisotropic triangular lattice with ring exchange model. We consider the classical phase diagrams for three variants of the ring exchange model III. In Sec. IV, we present the spin-wave theory formalism, while in Sec. V, we consider the ground-state properties: quantum phase diagram and staggered magnetization of the three models studied. In Sec. VI, we discuss the elementary excitations of the three models, in particular, (i) the existence of minima along the diagonal in the Néel phase and (ii) why the collinear phase is so fragile to quantum fluctuations. In Sec. VII, we relate our findings to the organic materials. Finally, in Sec. VIII, we present our conclusions.

II. HEISENBERG MODEL ON AN ANISOTROPIC TRIANGULAR LATTICE WITH RING EXCHANGE

We are interested in understanding the magnetic properties of the $S = 1/2$ multiple-spin exchange Hamiltonian [36,40] on an anisotropic triangular lattice involving ring exchange on

four sites at $T = 0$:

$$\hat{H} = \frac{J}{2}\sum_{\bullet\!-\!\bullet}\hat{P}_{ij} + \frac{J}{2}\sum_{\bullet\;\bullet}\hat{P}_{ij} + \frac{J'}{2}\sum_{\bullet\;\;\bullet}\hat{P}_{ij} + \frac{K}{S^2}\sum_{\square}(\hat{P}_{ijkl} + \hat{P}_{lkji}) + \frac{K'}{S^2}\sum_{\square}(\hat{P}_{ijkl} + \hat{P}_{lkji}) + \frac{K'}{S^2}\sum_{\square}(\hat{P}_{ijkl} + \hat{P}_{lkji}), \tag{1}$$

where J and J' measure the relative strengths of the nearest neighbor and next-nearest neighbor spin exchange, while K, and K' measure the relative strengths of the ring exchange terms on four-sites (since there are three ways to have four-site rings on the anisotropic triangular lattice c.f. Fig. 1). Note that we defined the ring exchange coupling constants K/S^2 and K'/S^2 to have a meaningful semiclassical limit for $S \to \infty$, i.e., so that the two-spin exchanges are not negligible with respect to the four-spin exchange terms in this limit. The permutation operator that exchanges two spins on sites i and j is given by $\hat{P}_{ij} = 2\mathbf{S}_i \cdot \mathbf{S}_j + \frac{1}{2}$ and $\hat{\mathbf{S}}_i$ is the usual spin operator on site i, while $\hat{P}_{ijkl} = \hat{P}_{ij}\hat{P}_{jk}\hat{P}_{kl}$ cyclically permutes four spins around a plaquette, cf. Fig. 1(b). At this point, it is helpful to note that, to lowest order in t/U and t'/U, $K'/K = J'/J$. In this work, we take this equality to hold, primarily to limit the size of the parameter space of the model.

III. CLASSICAL PHASE DIAGRAM

Writing out the Hamiltonian in terms of spin operators gives

$$\hat{H} = \hat{H}_2 + \hat{H}_2^* + \hat{H}_4. \tag{2}$$

The first term $\hat{H}_2$ arises from the usual Heisenberg exchange terms on the anisotropic triangular lattice:

$$\hat{H}_2 = J\sum_{\bullet\!-\!\bullet}\mathbf{S}_i \cdot \mathbf{S}_j + J\sum_{\bullet\;\bullet}\mathbf{S}_i \cdot \mathbf{S}_j + J'\sum_{\bullet\;\;\bullet}\mathbf{S}_i \cdot \mathbf{S}_j. \tag{3}$$

The next term $\hat{H}_2^*$ arises from the two-spin terms from the four-spin permutation operators. Physically it dresses the nearest-neighbor and next-nearest-neighbor exchange strengths and induces next-next nearest-neighbor contributions in the Heisenberg model:

$$\hat{H}_2^* = (2K + 3K')\sum_{\bullet\!-\!\bullet}\mathbf{S}_i \cdot \mathbf{S}_j + (2K + 3K')\sum_{\bullet\;\;\bullet}\mathbf{S}_i \cdot \mathbf{S}_j + (K + 4K')\sum_{\bullet\;\bullet}\mathbf{S}_i \cdot \mathbf{S}_j + K\sum_{\bullet\;\;\bullet}\mathbf{S}_i \cdot \mathbf{S}_j + K'\sum_{\bullet\;\;\bullet}\mathbf{S}_i \cdot \mathbf{S}_j + K'\sum_{\bullet\;\;\bullet}\mathbf{S}_i \cdot \mathbf{S}_j. \tag{4}$$

The final term consists of the four-spin plaquette terms on the anisotropic triangular lattice:

$$\hat{H}_4 = \frac{K}{S^2}\sum_{\square}\hat{T}_{ijkl} + \frac{K'}{S^2}\sum_{\square}\hat{T}_{ijkl} + \frac{K'}{S^2}\sum_{\square}\hat{T}_{ijkl}, \tag{5}$$

where

$$\hat{T}_{ijkl} = (\mathbf{S}_i \cdot \mathbf{S}_j)(\mathbf{S}_k \cdot \mathbf{S}_l) + (\mathbf{S}_i \cdot \mathbf{S}_l)(\mathbf{S}_j \cdot \mathbf{S}_k) - (\mathbf{S}_i \cdot \mathbf{S}_k)(\mathbf{S}_j \cdot \mathbf{S}_l). \tag{6}$$

We are interested in the relative effects of each of the terms in Eq. (2). We will therefore explicitly compare three models: (i) the full model given by Eq. (2), (ii) the extended Heisenberg model, $\hat{H}_{eH} = \hat{H}_2 + \hat{H}_2^*$, and finally (ii) the four-spin plaquette model $\hat{H}_P = \hat{H}_2 + \hat{H}_4$. From now on, these three models will be referred to as the "full," "extended Heisenberg," and "plaquette" models.

The four-spin terms in Eq. (6) are decoupled in a leading order mean-field approximation taking

$$\langle \mathbf{S}_\alpha \cdot \mathbf{S}_\beta \rangle = S^2 \cos(\mathbf{Q} \cdot \boldsymbol{\delta}_{\alpha\beta}), \tag{7}$$

so that

$$\frac{1}{S^2}(\mathbf{S}_\alpha \cdot \mathbf{S}_\beta)(\mathbf{S}_\gamma \cdot \mathbf{S}_\delta) = \cos(\mathbf{Q} \cdot \boldsymbol{\delta}_{\alpha\beta})\mathbf{S}_\gamma \cdot \mathbf{S}_\delta + \cos(\mathbf{Q} \cdot \boldsymbol{\delta}_{\gamma\delta})\mathbf{S}_\alpha \cdot \mathbf{S}_\beta - S^2 \cos(\mathbf{Q} \cdot \boldsymbol{\delta}_{\alpha\beta})\cos(\mathbf{Q} \cdot \boldsymbol{\delta}_{\gamma\delta}). \tag{8}$$

At this level of approximation, ring exchange contributes by dressing the effective two spin exchange and, in particular, introduces additional long-range frustrated interactions:

$$\begin{aligned} J_{\hat{\mathbf{x}}} &= J + 2K + 3K' + 2(K + K')\cos(Q_x) - K'\cos(Q_x + 2Q_y), \\ J_{\hat{\mathbf{y}}} &= J + 2K + 3K' + 2(K + K')\cos(Q_y) - K'\cos(2Q_x + Q_y), \\ J_{\hat{\mathbf{x}}+\hat{\mathbf{y}}} &= J' + K + 4K' + 4K'\cos(Q_x + Q_y) - K\cos(Q_x - Q_y), \\ J_{\hat{\mathbf{x}}-\hat{\mathbf{y}}} &= K[1 - \cos(Q_x + Q_y)], \\ J_{2\hat{\mathbf{x}}+\hat{\mathbf{y}}} &= K'[1 - \cos(Q_y)], \\ J_{\hat{\mathbf{x}}+2\hat{\mathbf{y}}} &= K'[1 - \cos(Q_x)], \end{aligned} \tag{9}$$

where $J_{\hat{\boldsymbol{\eta}}}$ describes an antiferromagnetic exchange interaction in the $\hat{\boldsymbol{\eta}}$ direction. Here, $\hat{\mathbf{x}}$ and $\hat{\mathbf{y}}$ are vectors of length one lattice spacing in the x and y directions respectively [cf. Fig. 1(a)]. All other $J_{\hat{\boldsymbol{\eta}}}$ are zero.

The classical ground-state energy per site for the full model is

$$\begin{aligned} \frac{E_{GS}^{(0)}}{NS^2} &= J[\cos(Q_x) + \cos(Q_y)] + J'\cos(Q_x + Q_y) \\ &\quad + K[1 + 2\cos(Q_x) + 2\cos(Q_y) \\ &\quad + 2\cos(Q_x)\cos(Q_y)] + K'[2 + 3\cos(Q_x) \\ &\quad + 3\cos(Q_y) + 4\cos(Q_x + Q_y) \\ &\quad + \cos(2Q_x + Q_y) + \cos(Q_x + 2Q_y)]. \end{aligned} \tag{10}$$

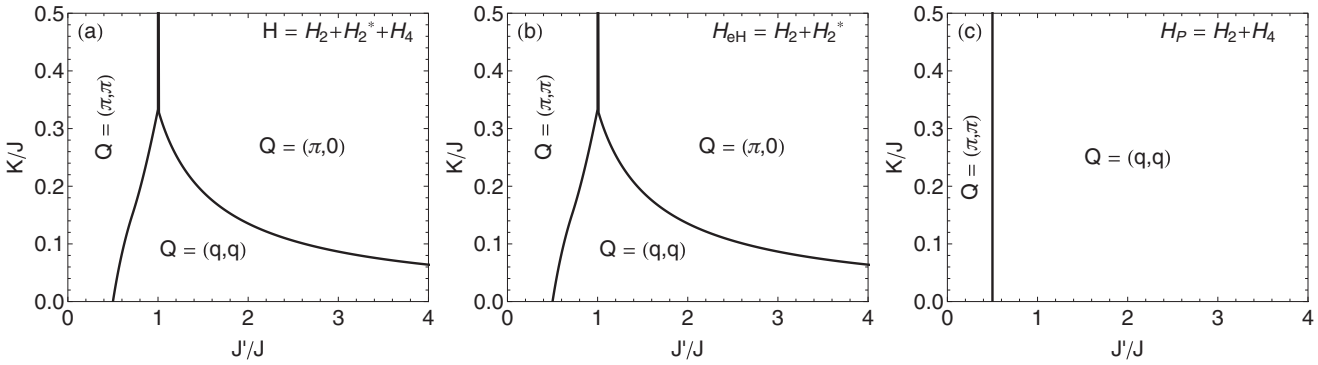

FIG. 2. Classical phase diagrams for the (a) full, (b) extended Heisenberg, and (c) plaquette models. The four-spin terms in the Hamiltonian, $\hat{H}_4$, contribute as trivial constants classically, resulting in the full and extended Heisenberg models having identical classical phase diagrams.

We note that the four-spin contribution [Eq. (5)] to the classical ground-state energy leads to a trivial constant $K + K'$ and the energies (and thence all other properties) of the full and extended Heisenberg models are identical.

To calculate the classical phase diagram, we considered Néel, collinear, and spiral phases with ordering vectors $\mathbf{Q} = (\pi,\pi)$, $\mathbf{Q} = (\pi,0)$, and $\mathbf{Q} = (q,q)$, respectively. We also considered several other phases including the diagonal, incommensurate spiral, columnar dimer and diagonal dimer phases with $\mathbf{Q} = (\pi/2,\pi/2)$, $\mathbf{Q} = (\pi,q)$, $\mathbf{Q} = (q-\pi,q)$, and $\mathbf{Q} = (\pi - 2q,q)$, respectively, when considering the classical phase diagram but these are all higher in energy. The ordering vector for the commensurate spiral phase q is found by minimizing Eq. (10) with respect to q assuming $Q_x = Q_y = q$. We find that the spiral ordering vector for the full and extended Heisenberg models depend on ring exchange, and are given by

$$q = \cos^{-1}\left[-\frac{J' + K + 4K' - \sqrt{(J' + K + 4K')^2 - 12(J + 2K)K'}}{12K'}\right], \tag{11}$$

whereas for the plaquette model we find

$$q = \cos^{-1}\left(-\frac{J}{2J'}\right). \tag{12}$$

In Fig. 2, we plot the classical phase diagrams obtained for the three models. For $K = 0$, we observe a transition from Néel to spiral order with $q = \cos^{-1}(-J/2J')$ for $J'/J = 0.5$, consistent with previous studies of the Heisenberg model [53,54]. With increasing ring exchange the Néel and collinear phases are stabilized, while the spiral order is destabilized in the full and extended Heisenberg models. Even at the classical level the spiral phase is most stable to ring exchange when $J' = J$. We will see below that this stabilisation of the spiral phase is reflected in the quantum calculations.

For the plaquette model, we find that the critical point between the Néel and spiral phases is independent of ring exchange classically since the ordering vector for the spiral phase in this model [Eq. (12)] is independent of ring exchange. The collinear phase is not observed in the plaquette models since it is always higher in energy than the spiral ordering.

IV. LINEAR SPIN-WAVE THEORY

We study the quantum phase diagram and elementary excitations for $S = 1/2$ at $T = 0$ using linear spin-wave theory. It is convenient [76,77] to assume that the spins lie in the x-z plane and rotate the quantum projection axis of the spins at each site along its classical direction:

$$\begin{aligned}\hat{S}_i^{x'} &= \tilde{S}_i^x \cos(\theta_i) + \tilde{S}_i^z \sin(\theta_i),\\ \hat{S}_i^{y'} &= \tilde{S}_i^y,\\ \hat{S}_i^{z'} &= -\tilde{S}_i^x \sin(\theta_i) + \tilde{S}_i^z \cos(\theta_i).\end{aligned} \tag{13}$$

Here, $\theta_i = \mathbf{Q}\cdot\mathbf{r}_i$, where $\mathbf{r}_i$ is the position of the i^{th} spin and $\mathbf{Q} = (Q_x, Q_y)$ is the ordering vector of the lattice. This simplifies the spin-wave treatment with the result that only one, rather than three, species of boson is required to describe the spin operators.

The bosonization of the spin operators is performed via the Holstein-Primakov transformation:

$$\begin{aligned}\tilde{S}_i^z &= S - \hat{a}_i^\dagger \hat{a}_i,\\ \tilde{S}_i^+ &= \sqrt{2S - \hat{a}_i^\dagger \hat{a}_i}\,\hat{a}_i,\\ \tilde{S}_i^- &= \hat{a}_i^\dagger \sqrt{2S - \hat{a}_i^\dagger \hat{a}_i},\end{aligned} \tag{14}$$

where $\tilde{S}_i^\pm = \tilde{S}_i^x \pm i\tilde{S}_i^y$ with subsequent expansion of square roots in powers of $a_i^\dagger a_i/(2S)$. Linear spin-wave theory takes the leading order terms in a $1/S$ expansion, which describe noninteracting spin waves. Performing a Fourier transform of the bosonic operators results in the following Hamiltonian:

$$\hat{H}_{\text{LSWT}} = 2S\sum_{\mathbf{k}}\left[A_{\mathbf{k}} a_{\mathbf{k}}^\dagger a_{\mathbf{k}} - \frac{B_{\mathbf{k}}}{2}(a_{\mathbf{k}}^\dagger a_{-\mathbf{k}}^\dagger + a_{\mathbf{k}} a_{-\mathbf{k}})\right], \tag{15}$$

where

$$A_{\mathbf{k}} = \sum_{\eta} \frac{J_\eta}{2} \cos(\mathbf{k}\cdot\boldsymbol{\delta}_\eta)[\cos(\mathbf{Q}\cdot\boldsymbol{\delta}_\eta)+1] - J_\eta \cos(\mathbf{Q}\cdot\boldsymbol{\delta}_\eta),$$
$$B_{\mathbf{k}} = \sum_{\eta} \frac{J_\eta}{2} \cos(\mathbf{k}\cdot\boldsymbol{\delta}_\eta)[1-\cos(\mathbf{Q}\cdot\boldsymbol{\delta}_\eta)], \tag{16}$$

Introducing the Fourier transform of the exchange interaction

$$J_{\mathbf{k}} = \sum_{\eta} J_\eta \cos(\mathbf{k}\cdot\boldsymbol{\delta}_\eta) \tag{17}$$

allows us to conveniently express the functions $A_{\mathbf{k}}$ and $B_{\mathbf{k}}$ through $J_{\mathbf{k}}$ as

$$A_{\mathbf{k}} = \frac{1}{4}(J_{\mathbf{Q}+\mathbf{k}} + J_{\mathbf{Q}-\mathbf{k}}) + \frac{J_{\mathbf{k}}}{2} - J_{\mathbf{Q}},$$
$$B_{\mathbf{k}} = \frac{J_{\mathbf{k}}}{2} - \frac{1}{4}(J_{\mathbf{Q}+\mathbf{k}} + J_{\mathbf{Q}-\mathbf{k}}). \tag{18}$$

We proceed by diagonalizing Eq. (15) via a Bogoliubov transformation

$$a_{\mathbf{k}}^\dagger = u_{\mathbf{k}}\alpha_{\mathbf{k}}^\dagger + v_{\mathbf{k}}\alpha_{-\mathbf{k}},$$
$$a_{\mathbf{k}} = u_{\mathbf{k}}\alpha_{\mathbf{k}} + v_{\mathbf{k}}\alpha_{-\mathbf{k}}^\dagger, \tag{19}$$

where

$$u_{\mathbf{k}} = \sqrt{\frac{A_{\mathbf{k}}}{\omega_{\mathbf{k}}} + \frac{1}{2}},$$
$$v_{\mathbf{k}} = \mathrm{sgn}(B_{\mathbf{k}})\sqrt{\frac{A_{\mathbf{k}}}{\omega_{\mathbf{k}}} - \frac{1}{2}}, \tag{20}$$

which yields

$$\hat{H} = E_{GS}^{(0)} + \frac{1}{2}\sum_{\mathbf{k}}(\omega_{\mathbf{k}} - A_{\mathbf{k}}) + \sum_{\mathbf{k}} \omega_{\mathbf{k}}\hat{\alpha}_{\mathbf{k}}^\dagger\hat{\alpha}_{\mathbf{k}}, \tag{21}$$

where the spin-excitation spectrum, $\omega_{\mathbf{k}}$, reads

$$\omega_{\mathbf{k}} = 2S\sqrt{(J_{\mathbf{k}} - J_{\mathbf{Q}})([J_{\mathbf{Q}+\mathbf{k}} + J_{\mathbf{Q}-\mathbf{k}}]/2 - J_{\mathbf{Q}})}. \tag{22}$$

It is already clear from Eq. (22) that the magnon spectrum has zeros at $\mathbf{k} = \mathbf{0}$ and $\mathbf{k} = \pm\mathbf{Q}$ in the two-dimensional Brillouin zone.

In studying the quantum phase diagram a key quantity is the staggered magnetization,

$$m_s = \langle \tilde{S}_i^z \rangle = S + \frac{1}{2} - \frac{1}{8\pi^2}\int_{\mathrm{BZ}} \frac{A_{\mathbf{k}}}{\omega_{\mathbf{k}}} d^2k \tag{23}$$

as m_s vanishes in a quantum disordered state.

V. GROUND-STATE PROPERTIES

A. Quantum phase diagrams

The quantum phase diagrams for the three models are shown in Fig. 3. All three models are equivalent for $K/J = K'/J = 0.0$. This model has been studied via LSWT previously [53,54]. As in these studies, we find a quantum critical point driven by the vanishing of the spin-wave velocity at $J'/J = 0.5$ and a quantum disordered phase for $J'/J \gtrsim 3.75$.

1. Full model

In the full model [Fig. 3(a)], ring exchange initially favours Néel order until the critical value of ring exchange, K_c, further increase of the ring-exchange coupling destabilizes Néel order. Similar behavior was observed by Majumdar *et al.* [72]. Interestingly, for $K < K_c$, the transition between the Néel and spin-liquid phases is second order, but for $K > K_c$, this transition is first order (cf. Figs. 4 and 5).

We also found that the spiral phase was dramatically suppressed in the quantum calculations compared to that found classically; the spiral phase only survives up to $K/J = 0.10$ for $J'/J = 1$ in contrast to $K/J = 1/3$, found classically. In a large region of the quantum phase diagram, the classically stable collinear phase is wiped out and replaced with a spin-liquid phase.

The behavior that we observe in the quantum phase diagram is highly analogous to the "order-by-disorder" mechanism due to quantum or thermal fluctuations [73–75,78]. In this mechanism, the fluctuations determine which ground states are stabilized and hence selected.

For the isotropic case ($J'/J = 1$), we found spiral order persists for $K/J < 0.1$. Previously Motrunich [32] predicted

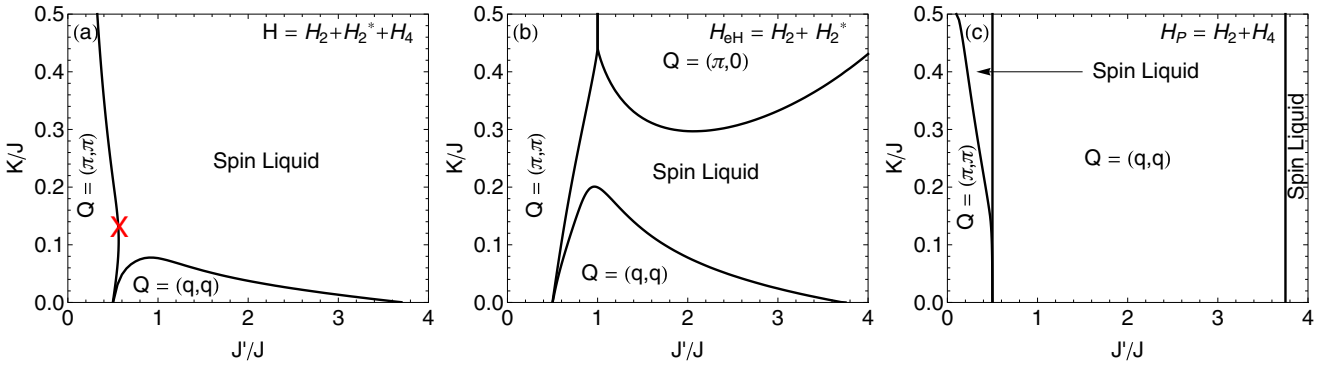

FIG. 3. (Color online) Quantum phase diagrams for (a) the full and extended Heisenberg models and (b) for the plaquette model. It is clear that, even in these semiclassical calculations, quantum fluctuations strongly suppress long-range order in the full and extended Heisenberg models when ring exchange is introduced. In addition, we have marked the critical end point where the staggered magnetization transitions from a second-order phase transition to a first-order phase transition with a red cross.

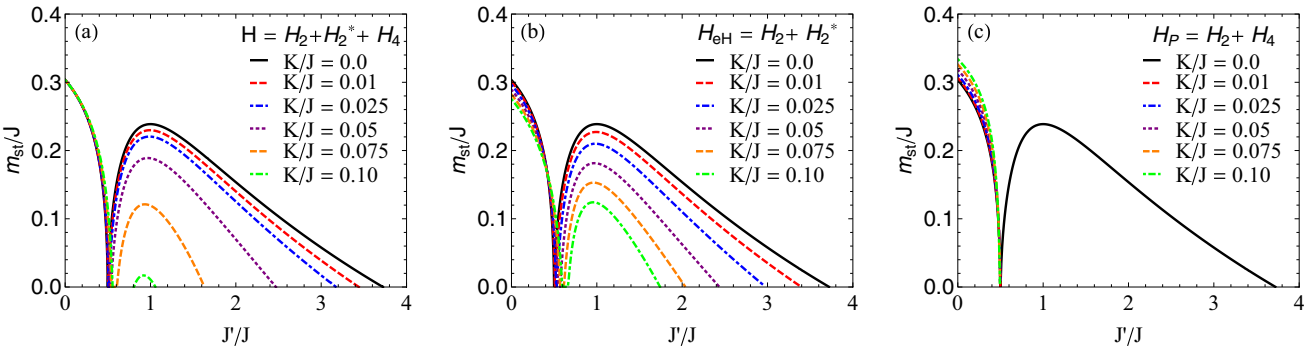

FIG. 4. (Color online) Staggered magnetization for the anisotropic triangular lattice with ring exchange calculated using linear spin-wave theory (LSWT). In each plot, we show the Néel-spiral transition for the (a) full, (b) extended Heisenberg, and (c) plaquette models. For the plaquette model (c), the magnetization is independent of ring-exchange for $J'/J > 0.5$ since the ordering vector in Eq. (12) is independent of ring exchange.

spiral order to be preserved for small $K/J \lesssim 0.14$–0.20 [34] but be destroyed for larger K/J leading to a gapped spin liquid for $K/J > 0.28$. Additionally, Kubo and Momoi considered numerous mean-field ground states with up to 144 sublattices [46]. In zero magnetic field, they found the spiral phase with 120° order exists for $K/J < 0.1$. Our results are consistent with both of these studies.

The most striking feature of the phase diagram is that, even in this semiclassical theory, quantum fluctuations destroy long-range magnetic order over large areas of the phase diagram. These quantum disordered regions occur in the parameter region consistent with DMRG calculations on four-leg triangular ladders [68].

2. *Extended Heisenberg and plaquette models*

For the extended Heisenberg model [Fig. 3(b)], we find that Néel order is stabilized by ring exchange and extends to the isotropic case ($J'/J = 1$) for $K/J \approx 0.44$ where it undergoes a first-order transition to the collinear phase. Additionally, we find that the spiral phase was suppressed in the quantum calculations relative to that found classically, although not as dramatically as in the full model. However, unlike the full model, the collinear phase is stable, although suppressed in the extended Heisenberg model. Furthermore, like the case for the full model, we found that the extended Heisenberg model also sustains a sizable spin-liquid phase. This is consistent with our recent Schwinger boson mean-field theory study of the effect of the third-nearest neighbor exchange terms on the magnetic properties of the anisotropic triangular lattice [71].

For the plaquette model in Fig. 3(c), we find that the Néel phase is stable for all $J'/J \leqslant 0.5$ up to $K/J \approx 0.1$, but further increasing ring exchange drives a quantum disordered phase for $J'/J \sim 0.5$. Additionally there is a spin-liquid phase for all $K/J \geqslant 0$ for $J'/J > 3.75$. For $0.5 < J'/J < 3.75$, spiral order is robust to ring exchange, as predicted classically.

Understanding the competing orders in both the extended Heisenberg and plaquette models is helpful in understanding the competing orders in the full model. The behavior of the Néel phase in the full model [see Fig. 3(a)] is as follows. For moderate values of K/J, the two-spin renormalization of the Heisenberg terms by ring exchange help stabilize Néel order, while for large values of K/J, the four-spin terms from ring exchange render the Néel phase unstable since such terms drive the development of a spin-liquid phase. The change in order of the Néel-spin-liquid phase transition is also consistent with this picture, as the phase transition remains second order in the extended Heisenberg model of all K, whereas this phase transition is always first order in the plaquette model. Similarly, the development of a large spin-liquid phase for large K/J in the full model can be understood from the two-spin ring contributions wanting to drive a collinear ground state, while the four-spin terms favor a spiral ground state.

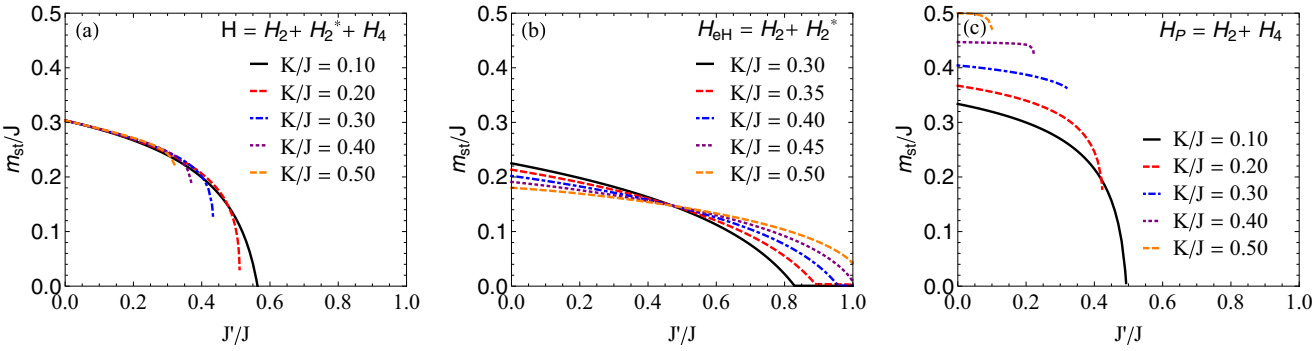

FIG. 5. (Color online) Staggered magnetization for the anisotropic triangular lattice with ring exchange calculated using linear spin-wave theory (LSWT). In each plot, we show the destabilization of Néel order for the (a) full, (b) extended Heisenberg, and (c) plaquette models.

B. Staggered magnetization

In Fig. 4(a), we present the staggered magnetization for the full model for the Néel and spiral phases as a function of J'/J for several values of K/J. The strong dip in the magnetization in the region 0.5–0.8 for the values of K/J considered, indicates a disordered intermediate phase. The nature of the ground state cannot be determined from linear spin-wave theory and will have to be determined by more sophisticated techniques.

Examination of the staggered magnetization in this parameter region indicates that both the Néel-spin-liquid and spiral-spin-liquid phase boundaries are lines of second-order phase transitions vanishing at a quantum critical point at $K = K' = 0$, $J'/J = 0.5$. This is consistent with what has previously been found in the $K = K' = 0$ case [53,54].

In Figs. 4(b) and 4(c), we present the staggered magnetization for the extended Heisenberg and plaquette models respectively for the Néel and spiral phases as a function of J'/J for several values of K/J. We observe that the two and four spin terms compete with each other with the former decreasing $m_{\rm st}$, while the latter increasing $m_{\rm st}$ with increasing K/J. This results in the negligible change in $m_{\rm st}$ in the Néel phase of the full model in Fig. 4(a). Furthermore, we observe the suppression of the spiral phase with increasing K/J is driven purely by the two-spin terms.

In Fig. 5, we present the staggered magnetization in the Néel phase for each of the three models. For the full and plaquette models, we observe that for small values of K/J the Néel order undegoes a second-order phase transition to the spiral phase [Figs. 5(a) and 5(c)], while for moderate K/J the transition from Néel order to the spin-liquid phase is clearly first order. Therefore the transition from enhancement to suppression of Néel order with increasing K/J can be understood in terms of a quantum critical endpoint being reached where the quantum phase transition changes from second to first order [marked by a red X in Fig. 3(a)]. For the extended Heisenberg model, we observe that for large K/J, the transition from Néel to collinear order is first order.

VI. SPIN-EXCITATION SPECTRA

We begin our discussion of the excitation spectra by considering the Néel phase. In the Néel phase of the full model, the antiferromagnetic exchange constants [Eq. (9)] reduce to

$$\begin{aligned} J_{\hat{\mathbf{x}}} &= J_{\hat{\mathbf{y}}} = J + 2K', \\ J_{\hat{\mathbf{x}}+\hat{\mathbf{y}}} &= J' + 8K', \\ J_{\hat{\mathbf{x}}-\hat{\mathbf{y}}} &= 0, \\ J_{2\hat{\mathbf{x}}+\hat{\mathbf{y}}} &= J_{\hat{\mathbf{x}}+2\hat{\mathbf{y}}} = 2K'. \end{aligned} \tag{24}$$

For the square lattice $K' = J' = 0$, since $K' = J'K$, the spin-wave dispersion is independent of the ring exchange coupling K in the full model, Eq. (1),

$$\begin{aligned} \omega_{\mathbf{k}}^2 = \{2J - J' + J[\cos(k_x) + \cos(k_y)] + J'\cos(k_x + k_y)\} \\ \times \{2J - J' - J[\cos(k_x) + \cos(k_y)] + J'\cos(k_x + k_y)\}. \end{aligned} \tag{25}$$

We plot this in Fig. 6.

In the plaquette model the antiferromagnetic exchange constants [Eq. (9)] in the Néel phase are

$$\begin{aligned} J_{\hat{\mathbf{x}}} &= J_{\hat{\mathbf{y}}} = J - 2K - K', \\ J_{\hat{\mathbf{x}}+\hat{\mathbf{y}}} &= J' + 4K' - K, \\ J_{\hat{\mathbf{x}}-\hat{\mathbf{y}}} &= 0, \\ J_{2\hat{\mathbf{x}}+\hat{\mathbf{y}}} &= J_{\hat{\mathbf{x}}+2\hat{\mathbf{y}}} = 2K'. \end{aligned} \tag{26}$$

However, the effect of ring exchange is opposite to that of the plaquette model, this results in the near independence of the spin-excitation spectrum observed of the full model to ring exchange observed in Fig. 6(a).

A. Excitation spectra for the full model

In Fig. 7(a), we plot the calculated spectra in the Néel phase for $J' = 0.5$. We find that increasing K/J leads to the softening of the mode at $\mathbf{k} = (\pi,0)$ and another along the diagonal $\mathbf{0}$-$\boldsymbol{\pi}$ direction, where $\mathbf{0} = (0,0)$ and $\boldsymbol{\pi} = (\pi,\pi)$. The later is more physically significant as it drives the Néel-spin-liquid transition. For sufficiently large K/J, local minima in $\omega_{\mathbf{k}}$ emerge at $\mathbf{k} = \mathbf{k_N} = (k_N,k_N)$ and $\mathbf{k} = \boldsymbol{\pi} - \mathbf{k_N}$ with

$$k_N = \arccos\left[\frac{\sqrt{(\kappa_1 - \sqrt{\kappa_2})/K'^2}}{8\sqrt{3}}\right], \tag{27}$$

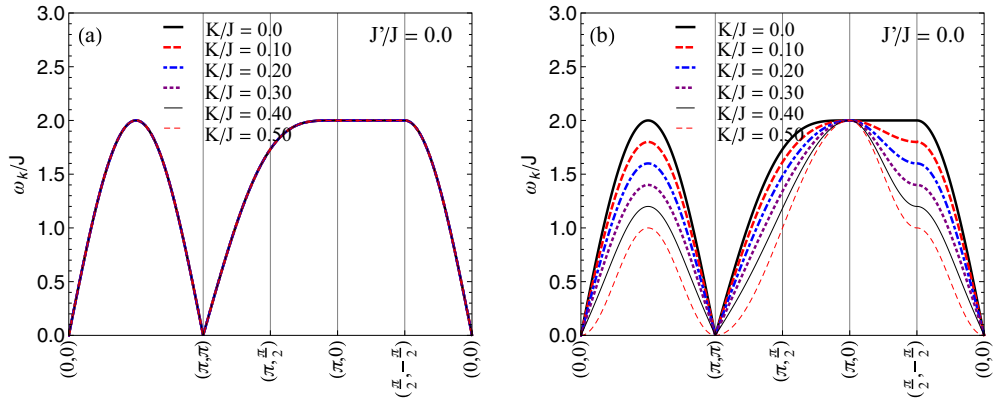

FIG. 6. (Color online) Comparison of spin-excitation spectrum on the square lattice obtained using (a) the full model $\hat{H} = \hat{H}_2 + \hat{H}_2^* + \hat{H}_4$ and (b) the plaquette model $\hat{H} = \hat{H}_2 + \hat{H}_4$.

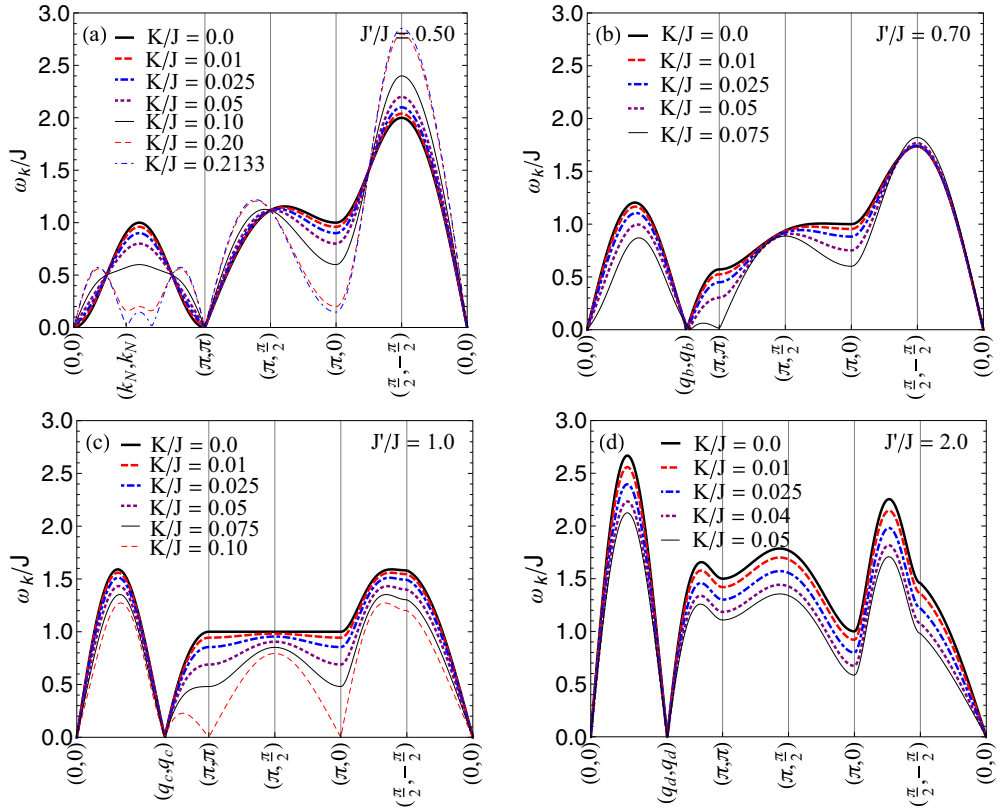

FIG. 7. (Color online) Spin-excitation spectra calculated for the full model for (a) the Néel phase with $J'/J = 0.5$ as well as for the commensurate spiral phase $J'/J = 0.7$ (b), $J'/J = 1.0$ (c), and $J'/J = 2.0$ (d). In (a)–(d), we mark spiral ordering vectors k_N, q_b, q_c, and q_d with $k_N \approx 0.40\pi$, $q_b \approx 0.76\pi$, $q_c = \frac{2}{3}\pi$, and $q_d \approx 0.58\pi$. In all cases, ring exchange increases the competition between the different classical phases, which causes a dramatic softening of the dispersion at the competing ordering wave vectors in (a)–(c). Above the critical value of the ring exchange, the dispersion becomes imaginary at these wave vectors—thus the competition between the different ordered phases is seen to be directly responsible for the quantum disordered phases.

where

$$\kappa_1 = J'^2 + 16K'(J' - J + 8K'),$$
$$\kappa_2 = J'^4 + 32K'[J'^3 - J'^2(J - 4K') - 4J'K'(J + 4K') + 2K'(J + 4K')^2]. \quad (28)$$

As K/J is further increased, these minima deepen and eventually $\omega_{\mathbf{k_N}} = \omega_{\boldsymbol{\pi}-\mathbf{k_N}}$ becomes imaginary ($\omega^2_{\mathbf{k_N}} < 0$). The softening of these modes can be understood by considering them to be massive modes with an "effective mass"

$$\frac{1}{m^*} = \left.\frac{\partial^2 \omega_{\mathbf{k}}}{\partial \mathbf{k}^2}\right|_{\mathbf{k}_0}, \quad (29)$$

where $\mathbf{k}_0$ is the momentum of the mode of interest, i.e., the momentum where the local minimum occurs. In Fig. 8, we plot the (a) gap and (b) effective mass of the $\mathbf{k} = (k_N,k_N)$ and $\mathbf{k} = (\pi,0)$ modes in the Néel phase for $J'/J = 0.5$ as functions of K/J. In calculating the effective masses we calculate the derivative along the $\mathbf{k} = (k,k)$ and $\mathbf{k} = (k_N/\sqrt{2} + k, k_N/\sqrt{2} - k)$ directions for the $\mathbf{k} = (k_N,k_N)$ mode. Similarly, for the $\mathbf{k} = (\pi,0)$ mode, we calculate the derivative along the (π,k) and (k,π) directions as well as along $(\pi/2 + k, \pi/2 - k)$ and $(\pi/2 + k, -\pi/2 + k)$ directions.

With increasing ring exchange we observe that the effective masses of both modes decrease. Eventually, the $\mathbf{k} = (k_N,k_N)$ mode becomes massless and Goldstone's theorem implies that the long-range order commensurate with that mode competes with the Néel phase. This leads to an instability of the Néel phase. This is a clear indication that Néel order has become unstable due to competition with the spiral phase. Explicit calculation shows that long range spiral order with $\mathbf{Q} = \mathbf{k_N}$ or $\boldsymbol{\pi} - \mathbf{k_N}$ is also unstable in this parameter regime. Generally, the instability of ordered phases for $K/J > 0$ results from the competition between two (or more) classical orders. It is the competition between Néel ($\mathbf{Q} = \boldsymbol{\pi}$) and spiral ($\mathbf{Q} = \mathbf{k_N}$) orders destroys the Néel long range order in the full model. This is very different from the mechanism for the vanishing of long range order at the quantum critical point in the $K = 0$ limit, which has been shown [53,54] to be due to the vanishing of the spin-wave velocity along $\mathbf{0}$-$\boldsymbol{\pi}$ and can be observed in Fig. 7(a).

In Figs. 7(b)–7(d), we plot the spectra in the spiral phase for $J' = 0.7$, J, and $2J$. In all three cases, one can clearly observe the expected Goldstone modes at $\mathbf{k} = \mathbf{0}$ and $\mathbf{k} = \mathbf{Q} = (q,q)$. In the spiral phase, increasing K/J induces softenings at $\mathbf{k} = \boldsymbol{\pi}$ and $\mathbf{k} = (\pi,0)$, i.e., at the momenta of the Goldstone modes of the Néel and collinear phases, respectively. For $J'/J = K'/K < 1$, the mode softens most rapidly at $\mathbf{k} = \boldsymbol{\pi}$. For sufficiently large K/J, we find that $\omega_{\boldsymbol{\pi}}$ becomes imaginary (as $\omega^2_{\boldsymbol{\pi}}$ becomes negative) indicating

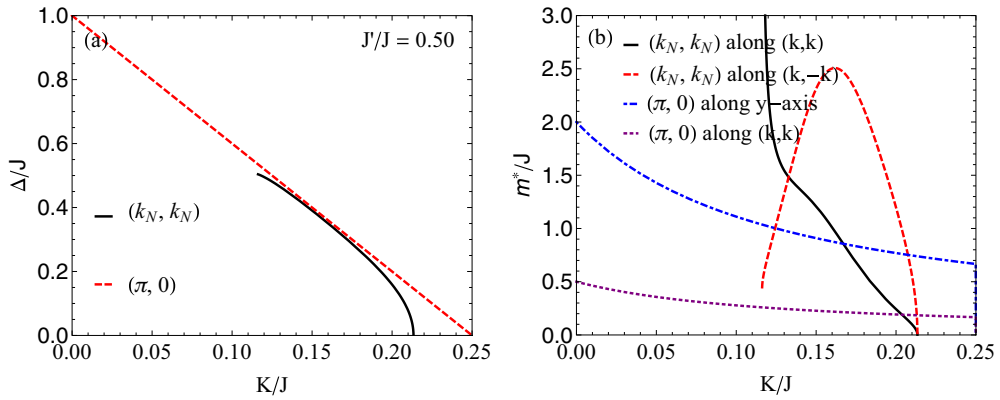

FIG. 8. (Color online) (a) Spin-wave gap and (b) effective masses for the Néel phase of the full model as functions of K/J for $J'/J = 0.5$. We consider both the $\mathbf{k} = \mathbf{k_N} = (k_N,k_N)$ and $\mathbf{k} = (\pi,0)$ modes as the compete with each other. In calculating the effective masses, we calculate the derivative along the diagonal $\mathbf{k} = (k,k)$ and perpendicular $\mathbf{k} = (k_N/\sqrt{2}+k, k_N/\sqrt{2}-k)$ directions for the $\mathbf{k} = (k_N,k_N)$ mode. These are shown by the black solid and red dashed curves respectively. Similarly for the $\mathbf{k} = (\pi,0)$ mode, we calculate the derivative along the boundary (π,k) and (k,π) directions as well as along the diagonal $(\pi/2+k,\pi/2-k)$ and $(\pi/2+k, -\pi/2+k)$ directions. These are shown by the blue dot-dashed and purple dotted curves, respectively.

that the competition with the Néel phase has destroyed the long-range spiral order. For $J'/J = K'/K > 1$, the mode softens most rapidly at $\mathbf{k} = (\pi,0)$. For sufficiently large K/J, we find that $\omega_{(\pi,0)}$ becomes imaginary indicating that the competition with the collinear phase has destroyed the long-range spiral order. At $J'/J = K'/K = 1$ [Fig. 7(c)] both the Néel and collinear phases compete with the spiral phases [as one would suspect from the classical phase diagram, Fig. 2(a)] and the dispersion becomes imaginary at $\mathbf{k} = \boldsymbol{\pi}$ and $\mathbf{k} = (\pi,0)$ simultaneously and likewise their effective masses also vanish simultaneously. A similar minimum at $(\pi,0)$ has been found from series expansions for the Heisenberg model on an anisotropic triangular lattice with no ring exchange due to recombination of particle-hole spinon pairs of momenta: $(\pi/2,\pi/2),(-\pi/2,-\pi/2)$ into magnons [12,56] in that case.

It is also interesting to note that for $J' = J$, the spiral order is more robust to the disordering effects induced by the ring exchange than for any other value of J'/J even classically. The effective two spin exchange couplings of Hamiltonian (1) are $\tilde{J}' = J' + K + 4K'$ and $\tilde{J} = J + 2K + 3K'$ implying that $\tilde{J}' = \tilde{J}$ for all K/J when $J'/J = K'/K = 1$. Furthermore, the strong geometrical frustration suppresses Néel and collinear phases thereby decreasing their ability to compete with spiral phase and drive an instability to the quantum spin liquid.

B. Absence of collinear phase in quantum calculations

We found that, in the parameter range covered by Fig. 2, the collinear phase is classically stable [see Fig. 2(a)]. However, in the quantum phase diagram [see Fig. 3(a)] the collinear phase is always unstable as there is always some point (or, typically, area) of the Brillouin zone for which $\omega_{\mathbf{k}}^2 < 0$. To demonstrate that the spectrum is unstable in the full model, we write down explicitly the expression for $\omega_{\mathbf{k}}^2$ assuming $\mathbf{Q} = (\pi,0)$ ordering:

$$\begin{aligned}\omega_{\mathbf{k}}^2 = &\{J' + [J + 4(K+K')]\cos(k_y)\}^2 \\ &- \{\cos(k_x)[J + 2K' + 4K\cos(k_y)] \\ &+ J'\cos(k_x+k_y) + 2K'\cos(k_x+2k_y)\}^2. \quad (30)\end{aligned}$$

In Fig. 9(a), we plot the minimum values (with respect to $\mathbf{k}$) of Eq. (30) and notice that $\min(\omega_{\mathbf{k}}^2) \leqslant -1$ for the entire parameter space considered. Therefore we conclude that competition with other classical phases means that the collinear phase is not stable in our calculations.

An important question to answer is why is the collinear phase so fragile in the quantum calculations for the full model. To address this, we consider explicit expressions for the spin-excitation spectrum in the collinear phase for the extended Heisenberg:

$$\begin{aligned}\omega_{\mathbf{k},\mathbf{eH}}^2 = &[J' + 2K + 4K' + (J + 2K + 3K')\cos(k_y) \\ &+ K'\cos(2k_x + k_y)]^2 - [(J + 2K + 3K')\cos(k_x) \\ &+ K\cos(k_x - k_y) + (J' + K + 4K')\cos(k_x + k_y) \\ &+ K'\cos(k_x + 2k_y)]^2 \quad (31)\end{aligned}$$

and plaquette models

$$\begin{aligned}\omega_{\mathbf{k},\mathbf{P}}^2 = &[J' - 2K - 4K' + (J + 2K + K')\cos(k_y) \\ &- K'\cos(2k_x + k_y)]^2 - [(J - 2K - K')\cos(k_x) \\ &+ K\cos(k_x - k_y) + (J' + K - 4K')\cos(k_x + k_y) \\ &+ K'\cos(k_x + 2k_y)]^2. \quad (32)\end{aligned}$$

We plot the values of the minima (with respect to $\mathbf{k}$) of Eqs. (31) and (32) in Figs. 9(b) and 9(c). There is a broad region of the phase diagram where the collinear phase is stable for the extended Heisenberg model but is unstable in the entire parameter space considered for the plaquette model. Therefore we conclude that it is the four-site ring exchange terms, rather than the renormalization of the exchange couplings that destabilizes the collinear phase.

One might wonder whether the instability of the collinear phase at harmonic order (leading order in $1/S$) in the spin-wave calculations is due to the spin waves in this phase not being properly described by this level of treatment. Hartree-Fock corrections, coming from the spin-wave interaction terms could stabilize the collinear phase. We have performed such a calculation but we find that the collinear phase is also unstable

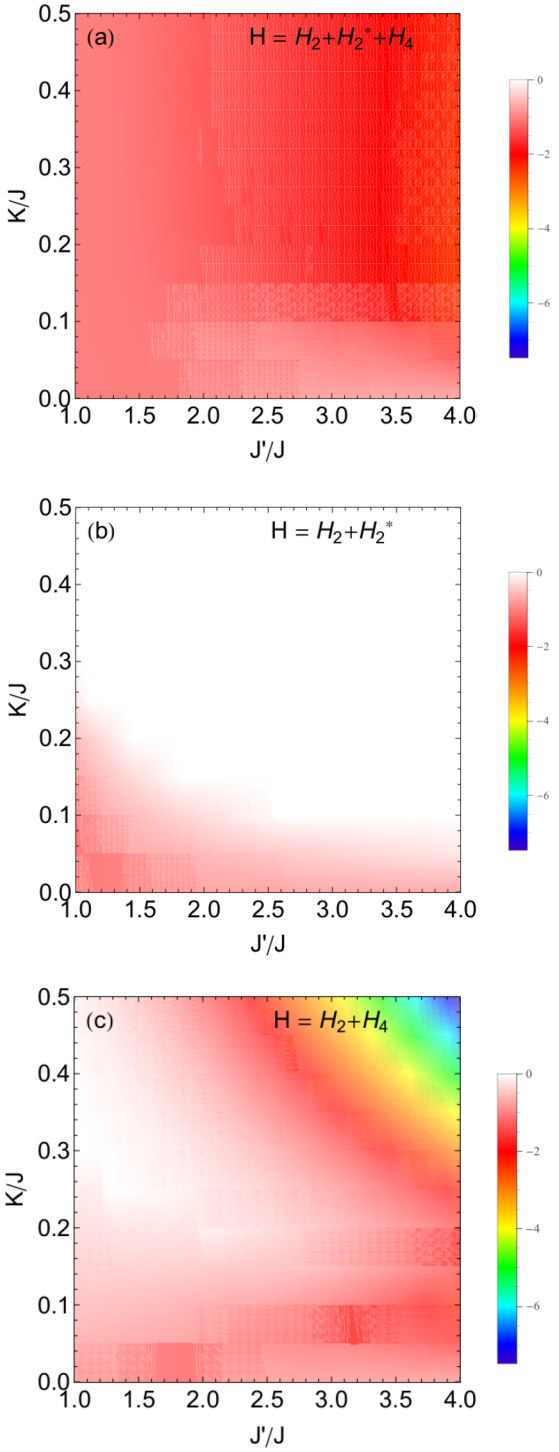

FIG. 9. (Color online) Minimum value of $\omega_{\mathbf{k}}^2$ assuming $\mathbf{Q} = (\pi,0)$ ordering. In (a), we use $\omega_{\mathbf{k}}^2$ obtained using the full model [Eq. (30)]; in (b), we use the spectrum calculated using the extended Heisenberg model [Eq. (31)]; while in (c), we use the spectrum calculated using the plaquette model [Eq. (32)]. Calculations were performed using LSWT.

for the full model with points (or regions) of the Brillouin zone where the renormalized spin excitation spectrum is imaginary. We will discuss this calculation in detail in a forthcoming manuscript, where we will calculate the full quantum phase diagram using Hartree-Fock mean-field theory.

VII. COMPARISON WITH ORGANICS

So far, we have limited the discussion to the spin degrees of freedom only. However, in the materials of interest, particularly the organic charge transfer salts, the charge degrees of freedom eventually become important and a Mott transition occurs under pressure. For $J' = J$ (120°), spiral order is found for $K/J \lesssim 0.1$. To lowest order $U/t = \sqrt{20J/K}$, which would suggest that the spiral-spin-liquid transition occurs at $U/t \simeq 14$, which is in good agreement with the previous calculations of Motrunich [32] and Yang *et al.* [33] for the isotropic triangular lattice model. This is also close to the estimated value of the critical ratio of U/t for the Mott transition on the triangular lattice [79]. This suggests that for $J' \sim J$, there is a direct transition from a spiral ordered Mott insulator to a metal as pressure is increased, which is believed to decrease U/t [3,8,80,81]. This is consistent with the observation [22] that organic charge transfer salts with $t' \simeq t$ undergo a Mott transition directly from a magnetically ordered phase to a superconducting/metallic phase, whereas salts with $J'/J \sim 0.8$ display spin-liquid (or other exotic quantum) phases.

In Fig. 10, we present a qualitative sketch of a proposed phase diagram for the Hubbard model on the anisotropic triangular lattice with ring exchange. The boundary lines for the Néel and spiral-ordered phases are based on the linear spin-wave theory for the full model, reported above. It is well known that the perfect nesting of the square lattice means that is insulating for arbitrarily small U/t. For $t' = t$, it is found, numerically, that the Mott transition occurs at around $U/t = 10$–15, depending on the method used [3,15–21,79]. The metal-insulator transition line in Fig. 10 is simply a smooth curve joining these points. Nevertheless, this simple analysis suggests that there will be a region of the phase diagram in the full model where the magnetic orderings compete strongly enough to induce a stable spin-liquid region. Comparing the observed phase diagrams of the κ-(BEDT-TTF)$_2X$ and Y[Pd(dmit)$_2$]$_2$ salts to this picture and taking into account the frustration (J'/J) estimated from first-principles calculations

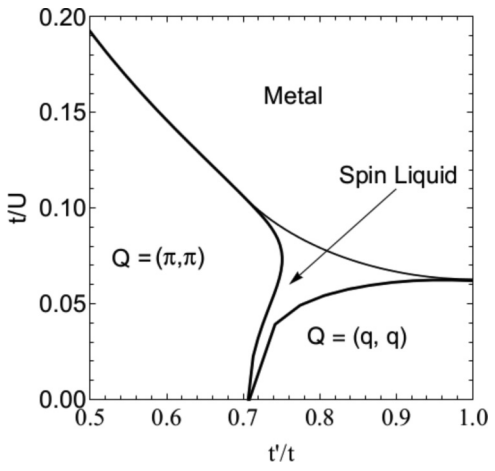

FIG. 10. Qualitative sketch of a proposed phase diagram for the Hubbard model on the anisotropic triangular lattice with ring exchange based on the LSWT calculations reported here and electronic structure calculations [22].

[22], one finds that this is consistent with what is observed experimentally.

VIII. CONCLUSIONS

In this paper, we have shown that the competition between different long-range order states creates a quantum disordered phase in the anisotropic triangular lattice Heisenberg model with ring exchange even at the semiclassical level. Analysis of the spin-wave spectra show that the spin-liquid state is a consequence of competition between classical ordered states. Thus we conclude that the interplay of ring exchange and geometrical frustration is responsible for the spin-liquid state found. Our results are relevant to weak Mott insulators, i.e., insulators lying close to the insulator-to-metal transition so that ring exchange is relevant. A future challenge is understanding ring exchange effects on two-dimensional metals close to the Mott transition which may lead to exotic non-Fermi liquid d-wave [82] phases.

ACKNOWLEDGMENTS

We thank Michel Gingras for helpful comments. This work was funded in part by the Australian Research Council under the Discovery (DP1093224), Future (FT130100161), and and QEII (DP0878523) schemes. J.M. acknowledges financial support from MINECO (MAT2012-37263-C02-01).

[1] L. Balents, Nature (London) **464**, 199 (2010).
[2] B. Normand, Contemp. Phys. **50**, 533 (2009).
[3] B. J. Powell and R. H. Mckenzie, Rep. Prog. Phys. **74**, 056501 (2011).
[4] P. A. Lee, Science **321**, 1306 (2008).
[5] Y. Shimizu, K. Miyagawa, K. Kanoda, M. Maesato, and G. Saito, Phys. Rev. Lett. **91**, 107001 (2003).
[6] S. Yamashita, Y. Nakazawa, M. Oguni, Y. Oshima, H. Nojiri, Y. Shimizu, K. Miygawa, and K. Kanoda, Nat. Phys. **4**, 459 (2008).
[7] M. Yamashita, N. Nakata, Y. Kasahara, T. Sasaki, N. Yoneyama, N. Kobayashi, S. Fujimoto, T. Shibauchi, and Y. Matsuda, Nat. Phys. **5**, 44 (2009).
[8] K. Kanoda and R. Kato, Annu. Rev. Condens. Matter Phys. **2**, 167 (2010).
[9] M. Yamashita, N. Nakata, Y. Senshu, M. Nagata, H. M. Yamamoto, R. Kato, T. Shibauchi, and Y. Matsuda, Science **328**, 1246 (2010).
[10] T. Itou, A. Oyamada, S. Maegawa, and R. Kato, Nat. Phys. **6**, 673 (2010).
[11] Y. Shimizu, H. Akimoto, H. Tsujii, A. Tajima, and R. Kato, J. Phys.: Condens. Matter **19**, 145240 (2007).
[12] J. O. Fjærestad, W. Zheng, R. R. P. Singh, R. H. McKenzie, and R. Coldea, Phys. Rev. B **75**, 174447 (2007).
[13] Y. Shirata, H. Tanaka, A. Matsuo, and K. Kindo, Phys. Rev. Lett. **108**, 057205 (2012).
[14] H. D. Zhou, E. S. Choi, G. Li, L. Balicas, C. R. Wiebe, Y. Qiu, J. R. D. Copley, and J. S. Gardner, Phys. Rev. Lett. **106**, 147204 (2011).
[15] J. Liu and J. Schmalian, and N. Trivedi, Phys. Rev. Lett. **94**, 127003 (2005).
[16] T. Watanabe, H. Yokoyama, Y. Tanaka, and J. Inoue, J. Phys. Soc. Jpn. **75**, 074707 (2006).
[17] P. Sahebsara and D. Senechal, Phys. Rev. Lett. **97**, 257004 (2006).
[18] B. Kyung and A. M. S. Tremblay, Phys. Rev. Lett. **97**, 046402 (2006).
[19] B. J. Powell and R. H. McKenzie, Phys. Rev. Lett. **98**, 027005 (2007).
[20] K. S. Chen, Z. Y. Meng, U. Yu, S. Yang, M. Jarrell, and J. Moreno, Phys. Rev. B **88**, 041103(R) (2013).
[21] L. F. Tocchio, H. Feldner, F. Becca, R. Valentí, and C. Gros, Phys. Rev. B **87**, 035143 (2013).
[22] E. P. Scriven and B. J. Powell, Phys. Rev. Lett. **109**, 097206 (2012).
[23] K. Nakamura, Y. Yoshimoto, T. Kosugi, R. Arita, and M. Imada, J. Phys. Soc. Jpn. **78**, 083710 (2009).
[24] H. C. Kandpal, I. Opahle, Y.-Z. Zhang, H. O. Jeschke, and R. Valenti, Phys. Rev. Lett. **103**, 067004 (2009).
[25] K. Nakamura, Y. Yoshimoto, and M. Imada, Phys. Rev. B **86**, 205117 (2012).
[26] T. Tsumuraya, H. Seo, M. Tsuchiizu, R. Kato, and T. Miyazaki, J. Phys. Soc. Jpn. **82**, 033709 (2013).
[27] T. Susuki, N. Kurita, T. Tanaka, H. Nojiri, A. Matsuo, K. Kindo, and H. Tanaka, Phys. Rev. Lett **110**, 267201 (2013).
[28] B. J. Powell and R. H. Mckenzie, J. Phys.: Condens. Matter **18**, R827 (2006).
[29] J. I. Yamaura, A. Nakao, and R. Kato, J. Phys. Soc. Jpn. **73**, 976 (2004).
[30] A. H. MacDonald, S. M. Girvin, and D. Yoshioka, Phys. Rev. B **37**, 9753 (1988).
[31] L. Balents and A. Paramekanti, Phys. Rev. B **67**, 134427 (2003).
[32] O. I. Motrunich, Phys. Rev. B **72**, 045105 (2005).
[33] H. Y. Yang, A. M. Lauchli, F. Mila, and K. P. Schmidt, Phys. Rev. Lett. **105**, 267204 (2010).
[34] Note in the convention followed in this paper J is a factor of two larger than in Ref. [32].
[35] M. Roger, J. H. Hetherington, and J. M. Delrieu, Rev. Mod. Phys. **55**, 1 (1983).
[36] D. J. Thouless, Proc. Phys. Soc. **86**, 893 (1965).
[37] H. Franco, R. E. Rapp, and H. Godfrin, Phys. Rev. Lett. **57**, 1161 (1986).
[38] H. Godfrin, R. R. Ruel, and D. D. Osheroff, Phys. Rev. Lett. **60**, 305 (1988).
[39] G. Misguich, B. Bernu, C. Lhuillier, and C. Waldtmann, Phys. Rev. Lett **81**, 1098 (1998).
[40] G. Misguich, C. Lhuillier, B. Bernu, and C. Waldtmann, Phys. Rev. B **60**, 1064 (1999).
[41] M. Roger, C. Bäerle, Yu. M. Bunkov, A. S. Chen, and H. Godfrin, Phys. Rev. Lett. **80**, 1308 (1998).
[42] K. Kubo and T. Momoi, Z. Phys. B **103**, 485 (1997).

[43] T. Momoi, K. Kubo, and K. Niki, Phys. Rev. Lett. **79**, 2081 (1997).
[44] K. Kubo, H. Sakamoto, T. Momoi, and K. Niki, J. Low. Temp. Phys. **111**, 583 (1998).
[45] T. Momoi, H. Sakamoto, and K. Kubo, Phys. Rev. B **59**, 9491 (1999).
[46] K. Kubo and T. Momoi, Physica B **329**, 142 (2003).
[47] C. Yasuda, D. Kinouchi, and K. Kubo, J. Phys. Soc. Jpn. **75**, 104705 (2006).
[48] S. Sugai, M. Sato, T. Kobayashi, J. Akimitsu, T. Ito, H. Takagi, S. Uchida, S. Hosoya, T. Kajitani, and T. Fukuda, Phys. Rev. B **42**, 1045 (1990).
[49] R. Coldea, S. M. Hayden, G. Aeppli, T. G. Perring, C. D. Frost, T. E. Mason, S. W. Cheong, and Z. Fisk, Phys. Rev. Lett. **86**, 5377 (2001).
[50] T. S. Nunner, P. Brune, T. Kopp, M. Windt, and Markus Grüninger, Phys. Rev. B **66**, 180404(R) (2002).
[51] P. W. Anderson, Mat. Res. Bull **8**, 153 (1973); P. Fazekas and P. W. Anderson, Philos. Magn. **30**, 423 (1974).
[52] P. Sindzingre, P. Lecheminant, and C. Lhuillier, Phys. Rev. B **50**, 3108 (1994).
[53] J. Merino, R. H. McKenzie, J. B. Marston, and C. H. Chung, J. Phys.: Condens. Matter **11**, 2965 (1999).
[54] A. E. Trumper, Phys. Rev. B **60**, 2987 (1999).
[55] P. Hauke, Phys. Rev. B **87**, 014415 (2013).
[56] W. Zheng, R. H. McKenzie, and R. R. P. Singh, Phys. Rev. B **59**, 14367 (1999).
[57] R. F. Bishop, P. H. Y. Li, D. J. J. Farnell, and C. E. Campbell, Phys. Rev. B **79**, 174405 (2009).
[58] C. H. Chung, J. B. Marston, and R. H. McKenzie, J. Phys.: Condens. Matter **13**, 5159 (2001).
[59] S. Yunoki and S. Sorella, Phys. Rev. B **74**, 014408 (2006); D. Heidarian, S. Sorella, and F. Becca, *ibid.* **80**, 012404 (2009).
[60] B. J. Powell and R. H. McKenzie, Phys. Rev. Lett. **94**, 047004 (2005).
[61] J. Y. Gan, Y. Chen, Z. B. Su, and F. C. Zhang, Phys. Rev. Lett. **94**, 067005 (2005).
[62] Y. Hayashi and M. Ogata, J. Phys. Soc. Jpn. **76**, 053705 (2007).
[63] J. Reuther and R. Thomale, Phys. Rev. B **83**, 024402 (2011).
[64] J. G. Rau and H.-Y. Kee, Phys. Rev. Lett. **106**, 056405 (2011).
[65] O. A. Starykh and L. Balents, Phys. Rev. Lett. **98**, 077205 (2007).
[66] M. Q. Weng, D. N. Sheng, Z. Y. Weng, and R. J. Bursill, Phys. Rev. B **74**, 012407 (2006); A. Weichselbaum and S. R. White, *ibid.* **84**, 245130 (2011).
[67] D. N. Sheng, O. I. Motrunich, and M. P. A. Fisher, Phys. Rev. B **79**, 205112 (2009).
[68] M. S. Block, D. N. Sheng, O. I. Motrunich, and M. P. A. Fisher, Phys. Rev. Lett. **106**, 157202 (2011).
[69] P. Hauke, T. Roscilde, V. Murg, J. Cirac, and R. Schmied, New J. Phys. **13**, 075017 (2011).
[70] H. Li, R. T. Clay, and S. Muzumdar, J. Phys.: Condens. Matter **22**, 272201 (2010).
[71] J. Merino, M. Holt, and B. J. Powell, arXiv:1402.3463.
[72] K. Majumdar, D. Furton, and G. S. Uhrig, Phys. Rev. B **85**, 144420 (2012).
[73] J. Villain, J. Phys. **38**, 385 (1977); J. Villain, R. Bidaux, J. P. Carton, and R. Conte, *ibid.* **41**, 1263 (1980).
[74] P. Chandra, P. Coleman, and A. I. Larkin, Phys. Rev. Lett. **64**, 88 (1990); J. Phys. Condens. Matter **2**, 7933 (1990).
[75] A. V. Chubukov and T. Jolicoeur, Phys. Rev. B **46**, 11137 (1992).
[76] S. Miyake, J. Phys. Soc. Jpn. **61**, 983 (1992).
[77] R. R. P. Singh and D. A. Huse, Phys. Rev. Lett. **68**, 1766 (1992).
[78] Q. Sheng and C. L. Henley, J. Phys. Condens. Matt. **4**, 2937 (1992).
[79] J. Merino, B. J. Powell, and R. H. McKenzie, Phys. Rev. B **73**, 235107 (2006); A. Liebsch, H. Ishida, and J. Merino, *ibid.* **79**, 195108 (2009).
[80] E. Scriven and B. J. Powell, J. Chem. Phys. **130**, 104508 (2009).
[81] E. Scriven and B. J. Powell, Phys. Rev. B **80**, 205107 (2009).
[82] H.-C. Jiang *et al.*, Nature (London) **493**, 39 (2012).